

LETTER

Kumdykolite, a high-temperature feldspar from an enstatite chondrite

PÉTER NÉMETH,<sup>1,2,\*</sup> STEPHEN W. LEHNER,<sup>2,3</sup> MICHAEL I. PETAEV,<sup>4</sup> AND PETER R. BUSECK<sup>2,3</sup>

<sup>1</sup>Institute of Materials and Environmental Chemistry, Research Center for Natural Sciences, Hungarian Academy of Sciences, H-1025 Budapest, Pusztaszeri út 59-67, Hungary

<sup>2</sup>School of Earth and Space Exploration, Arizona State University, Tempe, Arizona 85287-1404, U.S.A.

<sup>3</sup>Department of Chemistry and Biochemistry, Arizona State University, Tempe, Arizona 85287-1604, U.S.A.

<sup>4</sup>Department of Earth and Planetary Sciences, Harvard University, Solar, Stellar, and Planetary Sciences, Harvard-Smithsonian CfA, Cambridge, Massachusetts 02138, U.S.A.

ABSTRACT

We report the first occurrence of kumdykolite in a meteorite (Sahara 97072, EH3). This orthorhombic form of albite occurs in the core of a concentrically zoned metal-sulfide nodule. In contrast to the terrestrial kumdykolite, the meteoritic sample has a domain structure that is consistent with either orthorhombic ( $Pmnn$ ) or monoclinic ( $P2_1$ ) space groups. The two symmetries are indicated by the presence or lack, respectively, of  $h + k = 2n + 1$  reflections in  $[001]$  selected-area electron diffraction patterns, effects that likely result from different Si-Al ordering.  $Pmnn$  kumdykolite has only one tetrahedral site for Si and Al, whereas  $P2_1$  kumdykolite would have three tetrahedral sites for Si and one for Al. We propose that kumdykolite formed above 1300 K and cooled rapidly enough to preserve its unique structure. Apparently, the cooling rate varied on the scale of nanometers allowing the local development of Si-Al ordering.

**Keywords:** Kumdykolite, albite polymorph, enstatite chondrite, domain structure, Si-Al ordering

INTRODUCTION

Albite is an important Na-bearing mineral in unequilibrated, metal-rich enstatite (EH3) chondrites (Schneider et al. 2002; Lehner et al. 2013a), although it is rare in carbonaceous and ordinary chondrites. It is intimately intergrown with sulfides and silica produced through silicate sulfidation in EH3 chondrites (Lehner et al. 2013a, 2013b). Therefore, albite may carry important information about the sulfidation environment.

The albite structure has the potential to record thermal history (e.g., Smith 1974). At high temperature, it crystallizes with monoclinic symmetry. Below 1273 K, Si-Al ordering occurs (e.g., Salje 1985; Salje et al. 1989), which results in the triclinic high-albite structure. Upon cooling to below 973 K, the ordering leads to unit-cell distortion and formation of low albite (also triclinic). The known high-pressure (>10 GPa) albite polymorph is lingunite (Liu 1978; Liu and El Goresy 2007), with hollandite-type structure. Recently an albite polymorph with orthorhombic symmetry was described from eclogite in the ultrahigh-pressure Kumdy Kol, Kokchetav massif. The polymorph was named kumdykolite and proposed to be metastable, formed by rapid cooling from high temperature (Hwang et al. 2009).

We report the first occurrence of kumdykolite in a meteorite (SAH 97072 EH3). In contrast to the terrestrial example, this

kumdykolite has a domain structure and occurs in two forms with different Si-Al ordering. The goals of this paper are to describe its occurrence in an EH3 chondrite, discuss its crystal structure, Si-Al ordering, and its possible formation condition.

EXPERIMENTAL METHOD

Chemical analysis and backscattered electron (BSE) imaging of a concentrically zoned metal-sulfide nodule were performed using a thin section of SAH 97072 with an FEI NOVA scanning electron microscope (SEM). The Si- and Al-rich core of the nodule was extracted and thinned to electron transparency using a focused ion beam (FIB). Transmission electron microscope (TEM) data, bright-field TEM (BFTEM) images, and selected-area electron diffraction (SAED) patterns were acquired with JEOL2000FX and JEOL JEM 4000EX TEMs. The compositions of the grains were measured with an energy-dispersive X-ray spectrometer attached to a JEOL 2010F TEM. We used the Cliff-Lorimer thin-film approximation and ZAF correction to quantify the analysis using Genesis software. We used a  $\sim 0.1$   $\mu\text{m}$  electron beam and corrected the analyses for Na-loss by using an albite standard under identical conditions.

RESULTS

The nodule consists of a kamacite-troilite mantle and a core containing oldhamite, niningerite, Zn-daubreelite, and S-rich porous silica (Figs. 1a–1c). The porous silica contains grains of  $\text{NaAlSi}_3\text{O}_8$  (Table 1) that have SAED patterns consistent with kumdykolite (Figs. 2 and 3).

Kumdykolite was reported in space group  $Pmnn$  (Hwang et al. 2009), a symmetry that requires systematic absences for reflections with  $h + k = 2n + 1$  in SAED patterns along  $[001]$ . Patterns from some areas of the meteoritic kumdykolite are

\* E-mail: pnemeth1@asu.edu

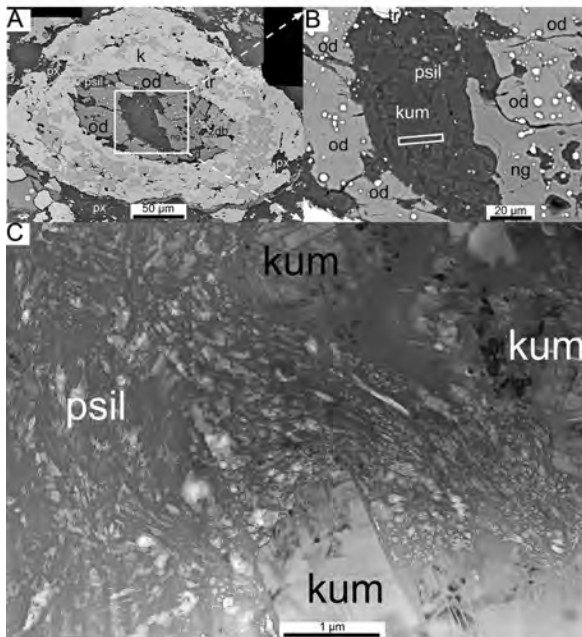


**FIGURE 1.** Petrographic setting of kumdykolite from EH3 chondrite SAH 97072. (a) BSE image of kumdykolite and S-rich porous silica at the center of a metal-sulfide nodule (Lehner et al. 2011). (b) Location of the FIB extraction (white rectangle). (c) BFTEM image of kumdykolite and porous silica. kum = kumdykolite, px = pyroxene, k = kamacite, ng = niningerite, od = oldhamite, psil = porous silica, tr = troilite, zdb = zincian daubreelite.

**TABLE 1.** Semi-quantitative chemical composition of kumdykolite

|                                | Spot 1 | Spot 2 | Spot 3 | Spot 4 | Spot 5 | Spot 6 |
|--------------------------------|--------|--------|--------|--------|--------|--------|
| SiO <sub>2</sub>               | 70.60  | 69.65  | 71.30  | 70.53  | 69.27  | 70.52  |
| Al <sub>2</sub> O <sub>3</sub> | 19.99  | 19.72  | 20.19  | 19.97  | 19.61  | 19.96  |
| Na <sub>2</sub> O              | 9.41   | 10.63  | 8.51   | 9.50   | 11.12  | 9.52   |
| <b>Based on 8 O</b>            |        |        |        |        |        |        |
| Si                             | 3.04   | 3.02   | 3.06   | 3.04   | 3.01   | 3.04   |
| Al                             | 1.01   | 1.01   | 1.02   | 1.02   | 1.00   | 1.01   |
| Na                             | 0.79   | 0.89   | 0.71   | 0.79   | 0.94   | 0.80   |
| Σ                              | 4.84   | 4.92   | 4.79   | 4.85   | 4.95   | 4.85   |

Notes: K and Ca were below the detection limit. The Na-content of <1 atom per formula unit points to Na-loss. The analytical error is estimated as  $\pm 5\%$ , relative.

consistent with these systematic absences (Figs. 2b, 2d, and 3b), but others display faint  $h + k = 2n + 1$  reflections (Figs. 2c and 3c) indicating that kumdykolite can occur with two symmetries. Diffraction of dynamically scattered electrons can result in reflections with  $h = 2n + 1$  along  $[100]^*$  and with  $k = 2n + 1$  along  $[010]^*$ . However,  $h + k = 2n + 1$  reflections with  $h \neq 0$  and  $k \neq 0$ , as observed in Figures 2c and 3c, cannot be interpreted as diffraction of dynamically scattered electrons, and, therefore, violate the selection rule for  $Pmnn$ . Multiple space groups are consistent with these SAED patterns (Figs. 2c and 3c). However, the patterns overlap for  $n$  glide reflections (the strong ones in Figs. 2c and 3c), indicating one may be a derivative symmetry of the other (Buerger 1947). Assuming the same unit cell, a possible derivative of  $Pmnn$  is  $P2_1$ , which is also the space group of the high-temperature synthetic anorthite published by Takeuchi et al. (1973) and sylvoslavite (Krivovichev et al. 2012). Based on these anorthite analogs, we propose that the space group of kumdykolite having  $h + k$

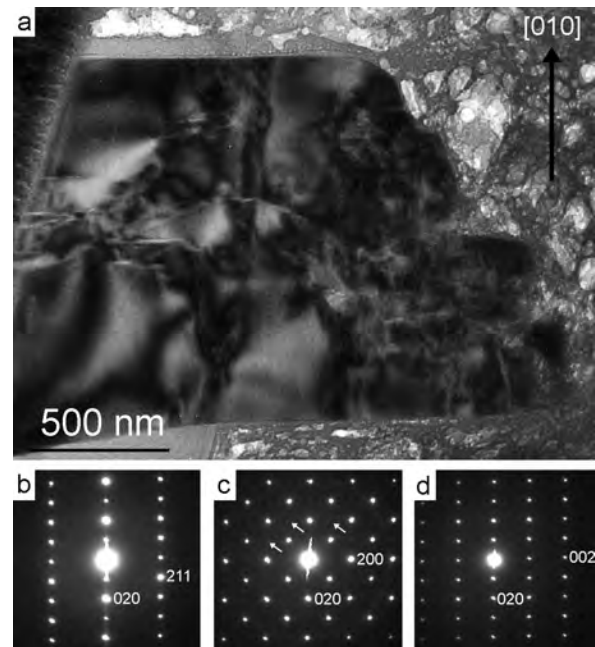


**FIGURE 2.** BFTEM image and SAED patterns of the kumdykolite grain (rotated clockwise  $110^\circ$ ) in the bottom center of Figure 1c. Reflections with  $h = 2n + 1$  along  $[100]^*$ , with  $k = 2n + 1$  along  $[010]^*$ , and with  $l = 2n + 1$  along  $[201]^*$  and  $[001]^*$  can occur because of diffraction of dynamically scattered electrons and are therefore not considered for the symmetry analysis. (a) Light and dark areas of the BFTEM image are indicative of antiphase domains. (b) SAED pattern along  $[102]$ . (c) SAED pattern along  $[001]$  tilted  $-40^\circ$  around  $[010]^*$  with respect to the pattern in panel b. Faint  $h + k = 2n + 1$  reflections (white arrows) violate the selection rule for  $Pmnn$ , but are consistent with  $P2_1$ . (d) SAED pattern along  $[100]$  tilted  $+50^\circ$  around  $[010]^*$  with respect to the pattern in panel b.

$= 2n + 1$  reflections is  $P2_1$ .

The occurrence of different space groups for the same mineral is common in feldspars and is indicated by  $a$ -,  $b$ -,  $c$ -, and  $d$ -type reflections in SAED patterns (Kroll and Ribbe 1980; Carpenter et al. 1985; Redfern 1992; Tribaudino and Angel 2012), as well as by antiphase domains and boundaries in TEM images (e.g., Carpenter 1991; Van Tendeloo et al. 1989; Németh et al. 2007). Therefore, we conclude that the dark and bright areas in kumdykolite BFTEM images (Figs. 2a and 3a) corresponding to SAED patterns with and without the  $h + k = 2n + 1$  reflections are antiphase domains and boundaries.

## DISCUSSION

### Structure and Si-Al ordering

The fractional coordinates for the Si-Al and O sites for  $Pmnn$  kumdykolite based on the Takeuchi et al. (1973) structure model for  $P2_1$  synthetic  $\text{CaAl}_2\text{Si}_2\text{O}_8$  were proposed by Hwang et al. (2009). They generated the coordinates for one Si-Al site and 3 O sites by shifting the origin in the  $P2_1$  structure and eliminating the equivalent positions. However, in this structure all O are in general positions, which results in unbalanced charge and 6-coordinated Si-Al. This problem can be solved if two O occupy special positions. Furthermore, following the method of

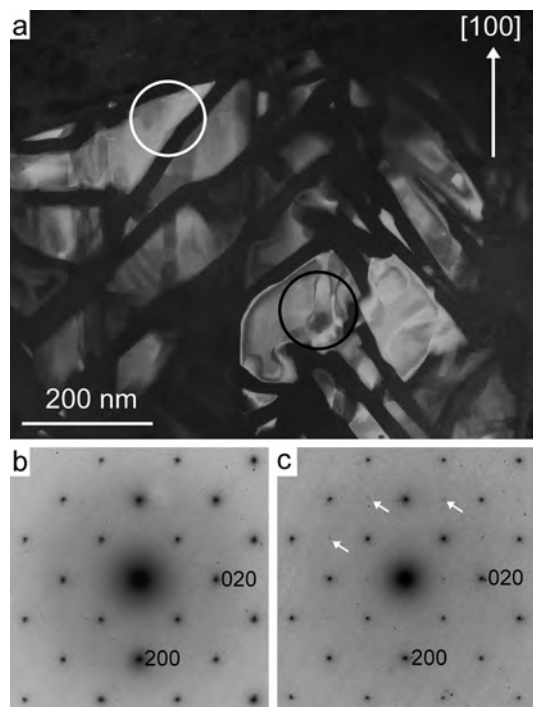


**FIGURE 3.** BFTEM image and SAED patterns of kumdykolite in the top center of Figure 1c. Reflections with  $h = 2n + 1$  along  $[100]^*$  and with  $k = 2n + 1$  along  $[010]^*$  in SAED patterns can occur because of diffraction of dynamically scattered electrons, and are therefore not considered for the symmetry analysis. (a) Areas of the BFTEM image with and without antiphase domains (black and white circles, respectively). The black stripes parallel to  $\langle 100 \rangle$  and  $\langle 110 \rangle$  are caused by amorphization. They increase in width with exposure to the electron beam. (b) SAED pattern along  $[001]$  from the area in the white circle in a shows only strong  $h + k = 2n$  reflections. (c) SAED pattern  $[001]$  from the area in the black circle of a shows faint  $h + k = 2n + 1$  reflections (white arrows) that violate the selection rule for  $Pmnn$  space group, but are consistent with  $P2_1$ .

**TABLE 2.** Atomic coordinates (CIF<sup>1</sup> available) for  $Pmnn$  kumdykolite derived from the structure of synthetic  $\text{CaAl}_2\text{Si}_2\text{O}_8$  given by Takeuchi et al. (1973)

| Atom | x      | y      | z      |
|------|--------|--------|--------|
| Na   | 0      | 0.4738 | 0.1142 |
| T    | 0.2003 | 0.1498 | 0.1445 |
| O1   | 0.3109 | 0.1819 | 0.4237 |
| O2   | 0.2880 | 0      | 0      |
| O3   | 0      | 0.1387 | 0.2521 |

Note: T is the tetrahedral site and can be occupied by Si or Al.

Hwang et al. (2009), a special Na site can be generated from the Takeuchi structure. Thus, we propose new atomic coordinates for  $Pmnn$  kumdykolite (Table 2) by modifying the structure of Hwang et al. (2009) and generating a Na site.

$Pmnn$  kumdykolite contains one framework cation site (Fig.

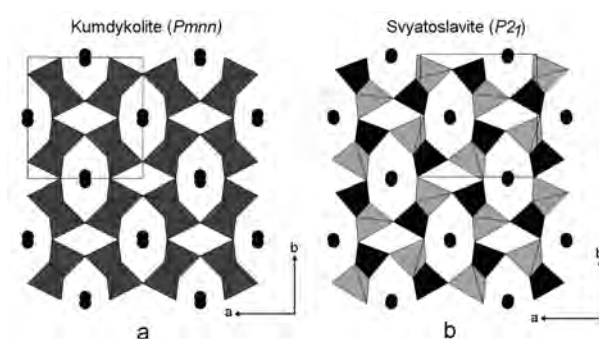


**FIGURE 4.** Crystal structures of  $Pmnn$  kumdykolite and  $P2_1$  svyatoslavite along  $[001]$ . Black rectangles outline the unit cells. The extra-framework cations (black balls) occur in split sites. (a) Kumdykolite in  $Pmnn$  space group has a disordered Si-Al framework as Si and Al are distributed in one site. Gray polyhedra represent both  $\text{SiO}_4$  and  $\text{AlO}_4$  tetrahedra. (b) Svyatoslavite in  $P2_1$  space group has an ordered Si-Al framework in which Si and Al occupy separate crystallographic sites. Black and light-gray polyhedra represent  $\text{SiO}_4$  and  $\text{AlO}_4$  tetrahedra, respectively.

4a), with a disordered distribution for Al and Si. However, the Na likely occupies a split site similar to Ca in the Takeuchi structure. We assume that  $P2_1$  kumdykolite contains ordered Si and Al in a structure analogous to that of synthetic  $P2_1$  anorthite and its natural analog, svyatoslavite (Takeuchi et al. 1973; Krivovichev et al. 2012). Although Si and Al ordering occurs via two Si and two Al sites in the Takeuchi structure (Fig. 4b), there would be one site for Al and three for Si in  $P2_1$  kumdykolite. By analogy to other feldspars, we presume that the low-symmetry kumdykolite structure develops during cooling.

### EH3 kumdykolite formation conditions

The kumdykolite molar volume ( $104 \text{ cm}^3/\text{mol}$ ) may provide an estimate of formation pressure. It is significantly greater than that of lingunite ( $70 \text{ cm}^3/\text{mol}$ ), the high-pressure albite polymorph, but similar to that of low albite ( $100 \text{ cm}^3/\text{mol}$ ). Therefore, we presume that kumdykolite did not form at high pressure.

The kumdykolite formation temperature can be postulated by comparison with the high-temperature  $\text{CaAl}_2\text{Si}_2\text{O}_8$  polymorphs svyatoslavite and dmisteinbergite and by considering the proposed conditions of silicate sulfidation in EH3 chondrites (Lehner et al. 2013b). Svyatoslavite and dmisteinbergite crystallize between 1373 and 1673 K (Abe et al. 1991; Abe and Sunagawa 1995) and have been used as indicators of rapid cooling (Sokol et al. 1998; Krivovichev et al. 2012; Nestola et al. 2010). Lehner et al. (2013a, 2013b) reported that  $\text{NaAlSi}_3\text{O}_8$  could form during sulfidation of Al-bearing pyroxenes through release of the  $\text{Al}_2\text{O}_3$  and  $\text{SiO}_2$  components in a Na-enriched environment. Thermodynamic modeling of phase relations indicates that silicate sulfidation occurred at  $\sim 1400$  to  $1600 \text{ K}$ , a range consistent with svyatoslavite crystallization. Therefore we propose that kumdykolite formed at high temperature, presumably  $>1300 \text{ K}$ , and cooled rapidly preserving its structure. Furthermore, Si-Al ordering and both high- and low-symmetry kumdykolite suggest the cooling rate varied on the scale of nanometers.

<sup>1</sup> Deposit item AM-13-065, CIF. Deposit items are available two ways: For a paper copy contact the Business Office of the Mineralogical Society of America (see inside front cover of recent issue) for price information. For an electronic copy visit the MSA web site at <http://www.minsocam.org>, go to the *American Mineralogist* Contents, find the table of contents for the specific volume/issue wanted, and then click on the deposit link there.

## ACKNOWLEDGMENTS

We thank I. Swainson, M. Tribaudino, and F. Nestola for careful reviews. We thank Jason Ng for preparing the FIB samples and are grateful to the staff of and facilities in the LeRoy Eyring Center for High Resolution Electron Microscopy at Arizona State University. P.N. acknowledges support from the Hungarian Scientific Research Fund and Hungarian Economic Development Centre grant HUMAN\_MB08-1-2011-0012. The work at ASU was supported by NASA grant NNX10AG48G.

## REFERENCES CITED

- Abe, T. and Sunagawa, I. (1995) Hexagonal  $\text{CaAl}_2\text{Si}_2\text{O}_8$  in a high temperature solution; metastable crystallization and transformation to anorthite. *Mineralogical Journal*, 17, 257–281.
- Abe, T., Tsukamoto, K., and Sunagawa, I. (1991) Nucleation, growth, and stability of  $\text{CaAl}_2\text{Si}_2\text{O}_8$  polymorphs. *Physics and Chemistry of Minerals*, 17, 473–484.
- Buerger, M.J. (1947) Derivative crystal structures. *Journal of Chemical Physics*, 15, 1–16.
- Carpenter, M.A. (1991) Mechanism and kinetics of Al-Si ordering in anorthite: I. Incommensurate structure and domain coarsening. *American Mineralogist*, 76, 1110–1119.
- Carpenter, M.A., McConnel, J.D.C., and Navrotsky, A. (1985) Enthalpies of ordering in the plagioclase feldspar solid solution. *Geochimica et Cosmochimica Acta*, 49, 947–966.
- Hwang, S.L., Shen, P.Y., Chu, H.T., Yui, T.F., Liou, J.G., and Sobolev, N.V. (2009) Kumdykolite, an orthorhombic polymorph of albite, from the Kokchetav ultrahigh-pressure massif, Kazakhstan. *European Journal of Mineralogy*, 21, 1325–1334.
- Krivovichev, S.V., Shcherbakova, E.P., and Nishanbaev, T.P. (2012) The crystal structure of svyatoslavite and evolution of complexity during crystallization of a  $\text{CaAl}_2\text{Si}_2\text{O}_8$  melt: A structural automata description. *Canadian Mineralogist*, 50, 585–592.
- Kroll, H. and Ribbe, P.H. (1980) Determinative diagrams for Al, Si order in plagioclases. *American Mineralogist*, 65, 449–457.
- Lehner, S.W., Petaev, M.I., Zolotov, M., and Buseck, P.R. (2011) Evidence for silicate sulfidation in EH3 metal-sulfide nodules. In Workshop on the formation of the first solids in the solar system. Lunar and Planetary Institute November 7–9, Kauai, Hawaii, Abstract 1863.
- Lehner, S.W., Nemeth, P., Petaev, M.I., and Buseck, P.R. (2013a) Origin of nanocrystalline albite in an EH3 sulfidized chondrule. 44<sup>th</sup> Lunar and Planetary Science conference, The Woodlands, Texas, Abstract 2500.
- Lehner, S.W., Petaev, M.I., Zolotov, M., and Buseck, P.R. (2013b) Formation of niningerite by silicate sulfidation in EH3 enstatite chondrites. *Geochimica et Cosmochimica Acta*, 101, 34–56.
- Liu, L. (1978) High-pressure phase transformations of albite, jadeite, and nepheline. *Earth and Planetary Science Letters*, 37, 438–444.
- Liu, L. and El Goresy, A. (2007) High-pressure phase transitions of the feldspars, and further characterization of lingunite. *International Geology Review*, 49, 854–860.
- Németh, P., Tribaudino, M., Bruno, E., and Buseck, P.R. (2007) TEM investigation of Ca-rich plagioclase: Structural fluctuations related to the  $\bar{1}\bar{1}-P\bar{1}$  phase transition. *American Mineralogist*, 92, 1080–1086.
- Nestola, F., Mitterpergher, S., Di Toro, G., Zorzi, F., and Pedron, D. (2010) Evidence of dmisteinbergite (hexagonal form of  $\text{CaAl}_2\text{Si}_2\text{O}_8$ ) in pseudotachylyte: A tool to constrain the thermal history of a seismic event. *American Mineralogist*, 95, 405–409.
- Redfern, S.A.T. (1992) The effect of Al/Si disorder on the  $\bar{1}\bar{1}-P\bar{1}$  co-elastic phase transition in Ca-rich plagioclase. *Physics and Chemistry of Minerals*, 19, 246–254.
- Salje, E. (1985) Thermodynamics of sodium-feldspar 1. Order parameter treatment and strain induced coupling effects. *Physics and Chemistry of Minerals*, 12, 93–98.
- Salje, E., Guttler, B., and Ormerod, C. (1989) Determination of the degree of Al, Si Order  $Q_{od}$  in kinetically disordered albite using hard mode infrared-spectroscopy. *Physics and Chemistry of Minerals*, 16, 576–581.
- Schneider, D.M., Symes, S.J.K., Benoit, P.H., and Sears, D.W.G. (2002) Properties of chondrules in EL3 chondrites, comparison with EH3 chondrites, and the implications for the formation of enstatite chondrites. *Meteoritics and Planetary Science*, 37, 1401–1416.
- Smith, J.V. (1974) *Feldspar Minerals*, vol. 1. Crystal structure and physical properties. Springer Verlag, Berlin.
- Sokol, E., Volkova, N., and Lepezin, G. (1998) Mineralogy of pyrometamorphic rocks associated with naturally burned coal-bearing spoil-heaps of the Chelyabinsk coal basin, Russia. *European Journal of Mineralogy*, 10, 1003–1014.
- Takeuchi, Y., Haga, N., and Ito, J. (1973) Crystal-structure of monoclinic  $\text{CaAl}_2\text{Si}_2\text{O}_8$ : a case of monoclinic structure closely simulating orthorhombic symmetry. *Zeitschrift für Kristallographie*, 137, 380–398.
- Tribaudino, M. and Angel, R. (2012) The thermodynamics of the  $\bar{1}\bar{1}-P\bar{1}$  phase transition in Ca-rich plagioclase from an assessment of the spontaneous strain. *Physics and Chemistry of Minerals*, 39, 699–712.
- Van Tendeloo, G., Ghose, S., and Amelinckx, S. (1989) A dynamical model for the  $P\bar{1}-\bar{1}\bar{1}$  phase transition in anorthite,  $\text{CaAl}_2\text{Si}_2\text{O}_8$ . *Physics and Chemistry of Minerals*, 16, 311–319.

MANUSCRIPT RECEIVED JANUARY 8, 2013

MANUSCRIPT ACCEPTED JANUARY 29, 2013

MANUSCRIPT HANDLED BY IAN SWAINSON

# Nemeth et al.: Supplemental Data, AM-13-065: American Mineralogist MayJune 2013

# This file was generated by ISOCIF, version 2.3.5  
# Harold T. Stokes and Branton J. Campbell  
# Brigham Young University, Provo, Utah, USA  
#  
# Model proposed for Pmnn kumdykolite modifying the structure of Hwang, S.L., Shen, P.Y., Chu, H.T., Yui, T.F., Liou, J.G., and Sobolev, N.V. (2009)  
# Kumdykolite, an orthorhombic polymorph of albite, from the Kokchetav ultrahigh-pressure massif, Kazakhstan.  
# European Journal of Mineralogy, 21, 1325-1334 to account for charge balance.  
# The atomic coordinates are derived from the structure of synthetic CaAl<sub>2</sub>Si<sub>2</sub>O<sub>8</sub> given by Takeuchi, Y., Haga, N., and Ito, J. (1973)  
# Crystal-structure of monoclinic CaAl<sub>2</sub>Si<sub>2</sub>O<sub>8</sub>- a case of monoclinic structure closely simulating orthorhombic symmetry.  
# Zeitschrift für Kristallographie, 137, 380-398.  
# The T site contains disordered Si and Al in the proportion AlSi<sub>3</sub>.  
# Na is in split site.

data\_isocif-output  
\_audit\_creation\_method ISOCIF  
\_symmetry\_space\_group\_name\_H-M "P 2/m 21/n 21/n"  
\_symmetry\_Int\_Tables\_number 58  
\_cell\_length\_a 8.24000  
\_cell\_length\_b 8.68000  
\_cell\_length\_c 4.84000  
\_cell\_angle\_alpha 90.00000  
\_cell\_angle\_beta 90.00000  
\_cell\_angle\_gamma 90.00000

loop\_  
\_space\_group\_symop\_id  
\_space\_group\_symop\_operation\_xyz  
1 x,y,z  
2 -x+1/2,y+1/2,-z+1/2  
3 -x+1/2,-y+1/2,z+1/2  
4 x,-y,-z  
5 -x,-y,-z  
6 x+1/2,-y+1/2,z+1/2  
7 x+1/2,y+1/2,-z+1/2  
8 -x,y,z

loop\_  
\_atom\_site\_label  
\_atom\_site\_type\_symbol  
\_atom\_site\_symmetry\_multiplicity  
\_atom\_site\_Wyckoff\_label  
\_atom\_site\_fract\_x  
\_atom\_site\_fract\_y  
\_atom\_site\_fract\_z  
\_atom\_site\_occupancy  
Na Na 4 g 0.00000 0.47380 0.11420 1.00000  
T T 8 h 0.20030 0.14980 0.14450 1.00000  
O1 O 8 h 0.31090 0.18190 0.42370 1.00000

O2 O 4 e 0.28800 0.00000 0.00000 1.00000  
O3 O 4 g 0.00000 0.13870 0.25210 1.00000